

Blood vessel tissue prestress modeling for vascular fluid–structure interaction simulation

Ming-Chen Hsu^{a,*}, Yuri Bazilevs^a

^a*Department of Structural Engineering, University of California, San Diego, 9500 Gilman Drive, Mail Code 0085, La Jolla, CA 92093, USA*

Abstract

In this paper we present a new strategy for obtaining blood vessel tissue prestress for use in fluid–structure interaction (FSI) analysis of vascular blood flow. The method consists of a simple iterative procedure and is applicable to a large class of vascular geometries. The formulation of the solid problem is modified to account for the tissue prestress by employing an additive decomposition of the second Piola–Kirchhoff stress tensor. Computational results using patient-specific models of cerebral aneurysms indicate that tissue prestress plays an important role in predicting hemodynamic quantities of interest in vascular FSI simulations.

Keywords: Blood vessels, Tissue prestress, Cerebral aneurysms, Fluid–structure interaction, Wall shear stress, Wall tension

1. Introduction

In recent years, a considerable effort was put forth to apply computational techniques to study and classify flow patterns and hemodynamic quantities of interest in a large sample of patient-specific cerebral aneurysm shapes. These results, practically unattainable in experiments or measurements, are connected to clinical events, which help better understand the disease processes and improve patient evaluation and treatment. The most studied quantity is the wall shear stress (WSS), which is connected with origination and progression of cardiovascular disease [1, 2]. For example, the high WSS may have important effects to the formation of aneurysms [3–5], while the low WSS may lead to the growth and rupture of them [6–8]. Such hemodynamic quantities of interest are typically obtained from pure computational fluid dynamics (CFD) simulations, mainly due to easy access to the commercial and research software. However, in many recent works [9–27], it has been shown that the elastic motion of the arterial wall has a significant effect on the hemodynamic quantities of interest. In particular, the rigid wall assumption (i.e. pure CFD modeling) overestimates WSS, precludes pressure wave propagation in blood vessels,

*Corresponding author

Email address: m5hsu@ucsd.edu (Ming-Chen Hsu)

and, most importantly, disregards stresses in the wall tissue. Wall tissue stress information is critical for the assessment of rupture risk, because rupture occurs when wall stress exceeds its strength [28, 29]. As a result, in order to determine accurate criteria for predicting aneurysm formation, growth and rupture, it is important to model vascular flow in conjunction with vessel wall deformation, which leads to coupled fluid–structure interaction (FSI) modeling.

The mechanical behavior of blood vessel tissue is well described by means of large-deformation three-dimensional solid or shell modeling [30, 31]. A total Lagrangian formulation with a hyperelastic constitutive law is typically employed. In hyperelasticity, the formulation relies on the existence of a unique stress-free configuration, which acts as a reference or initial configuration from which the displacement vector is computed. In vascular FSI analysis, patient-specific geometries of blood vessels are obtained from medical imaging data. When imaged, the blood vessels are in a state of mechanical stress that puts them in equilibrium with loading coming from the blood flow (i.e. blood pressure and viscous traction). As a result, when modeling blood vessel tissue, a patient-specific geometry configuration coming from imaging data may not be used as a stress-free configuration.

This problem was partially addressed in recent works. Tezduyar et al. [32] and Takizawa et al. [22] proposed a method of obtaining an estimated zero-pressure geometry. This estimated geometrical configuration is then used as a stress-free initial configuration in FSI simulations. However, the proposed procedure gives a resultant stressed configuration that is only a close approximation of the patient-specific geometry coming from imaging data. Gee et al. [33, 34] developed a modified updated Lagrangian formulation (MULF), which uses an incremental procedure to obtain an effective deformation gradient from an unknown reference configuration. The computed deformation gradient is used to determine the prestrained/prestressed state of the system. However, no discussion is given in [33, 34] regarding applications of the proposed methodology to dynamics and FSI. In this work, we take a different approach. We first directly compute the state of prestress in the blood vessel using an iterative procedure. We then modify the solid formulation to incorporate the prestress directly using the additive decomposition of the second Piola–Kirchhoff stress tensor.

We did not attempt to compute a stress-free configuration using the inverse motion strategy of Govindjee and Mihalic [35], because as observed in [33] for abdominal aortic aneurysm (AAA) simulations driven by intramural pressure, this configuration is usually not unique, or may not exist at all. The non-uniqueness of the stress-free configuration has been demonstrated in [35] when the strategy is applied to the full set of nonlinear elasticity equations. The nonexistence may be related to the fact that blood vessel formation involves not just deformation due of mechanical forces. A large role in this is played by the tissue growth and remodeling processes, which take place at the cell level and constantly change the material composition of blood vessels [36–38].

The paper is organized as follows. In Section 2, we give the formulation of the

tissue prestress problem and propose an iterative procedure for obtaining the tissue prestress tensor. We then describe our vascular FSI framework at the continuous and discrete levels in which we explicitly account for the tissue prestress. In Section 3, we present numerical examples of patient-specific cerebral aneurysms in which we compare FSI results with and without tissue prestress. In Section 4, we draw conclusions.

2. Vascular fluid–structure interaction simulation

2.1. Conventional variational formulation of the solid problem

Let \mathbf{X} be the coordinates of the initial or reference configuration, which is stress free, and let \mathbf{u} be the displacement with respect to the reference configuration. The coordinates of the current configuration, \mathbf{x} , are given by

$$\mathbf{x} = \mathbf{X} + \mathbf{u}. \quad (1)$$

The deformation gradient tensor \mathbf{F} is defined as

$$\mathbf{F} = \frac{\partial \mathbf{x}}{\partial \mathbf{X}} = \mathbf{I} + \frac{\partial \mathbf{u}}{\partial \mathbf{X}}, \quad (2)$$

where \mathbf{I} is the identity tensor.

Let \mathcal{V}^s and \mathcal{W}^s be the trial solution and weighting function spaces for the solid problem. The blood vessel tissue is modeled as a three-dimensional hyperelastic solid and the variational formulation which represents the balance of linear momentum for the solid is stated as follows: Find the displacement $\mathbf{u} \in \mathcal{V}^s$, such that for all weighting functions $\mathbf{w} \in \mathcal{W}^s$,

$$\left(\mathbf{w}, \rho_0 \frac{\partial^2 \mathbf{u}}{\partial t^2} \right)_{\Omega_0^s} + (\nabla_X \mathbf{w}, \mathbf{F} \mathbf{S})_{\Omega_0^s} = (\mathbf{w}, \rho_0 \mathbf{f})_{\Omega_0^s} + (\mathbf{w}, \mathbf{h})_{\Gamma_0^{s,N}}, \quad (3)$$

where Ω_0^s is the solid domain in the reference configuration, $\Gamma_0^{s,N}$ is the Neumann part of the solid boundary, ρ_0 is the density of the solid in the reference configuration, ∇_X is the gradient operator on Ω_0^s , \mathbf{f} and \mathbf{h} are the body force and surface traction, respectively.

In (3), \mathbf{S} is the second Piola–Kirchhoff stress tensor that derives from the gradient of an elastic stored energy function and is given by

$$\mathbf{S} = \mu^s J^{-2/3} \left(\mathbf{I} - \frac{1}{3} \text{tr} \mathbf{C} \mathbf{C}^{-1} \right) + \frac{1}{2} \kappa^s (J^2 - 1) \mathbf{C}^{-1}. \quad (4)$$

In the above, μ^s and κ^s are interpreted as the blood vessel shear and bulk moduli, respectively, $J = \det \mathbf{F}$ is the Jacobian determinant, and $\mathbf{C} = \mathbf{F}^T \mathbf{F}$ is the Cauchy–Green deformation tensor.

The material model in (4) may be found in Simo and Hughes [39], and its stress–strain behavior was analytically studied on simple cases of uniaxial strain [17] and

pure shear [40]. The model was argued to be appropriate for cerebral aneurysm FSI simulations in [25]. In particular, it was shown in [25], that the level of elastic strain in these problems is sufficiently large to preclude the use of infinitesimal (linear) strains, yet not large enough to be sensitive to the nonlinearity of the particular material model. Moreover, the current model has the advantage of stable behavior for the regime of strong compression, which may be present in the regions of arterial branching (see, e.g. [17]).

2.2. Tissue prestress problem

The formulation (3) assumes the reference configuration to be stress free. However, the blood vessel configuration coming from imaging data is typically not stress free. It is subjected to blood pressure and viscous traction and develops an internal stress state to resist these external loads. To account for this, we propose to modify the variational formulation (3) as follows: Find \mathbf{u} , such that for all \mathbf{w} ,

$$\left(\mathbf{w}, \rho_0 \frac{\partial^2 \mathbf{u}}{\partial t^2} \right)_{\Omega_0^s} + (\nabla_X \mathbf{w}, \mathbf{F}(\mathbf{S} + \mathbf{S}_0))_{\Omega_0^s} = (\mathbf{w}, \rho_0 \mathbf{f})_{\Omega_0^s} + (\mathbf{w}, \mathbf{h})_{\Gamma_0^{fs}}. \quad (5)$$

The modification consists of adding an a priori specified prestress tensor \mathbf{S}_0 . The prestress tensor is designed such that in the absence of displacement the blood vessel is in equilibrium with the blood flow forces. This design condition leads to the following variational problem, obtained by setting displacement to zero in (5): Find the symmetric prestress tensor \mathbf{S}_0 , such that for all vector-valued test functions \mathbf{w} ,

$$(\nabla_X \mathbf{w}, \mathbf{S}_0)_{\Omega_0^s} + (\mathbf{w}, \tilde{\mathbf{h}})_{\Gamma_0^{fs}} = 0. \quad (6)$$

In the above, Ω_0^s is the blood vessel reference configuration coming from imaging data, Γ_0^{fs} is the fluid–solid boundary in the reference configuration, and $\tilde{\mathbf{h}}$ is the fluid traction vector. The fluid traction vector $\tilde{\mathbf{h}}$ may be obtained from a separate rigid-wall blood flow simulation on the reference domain with steady inflow and resistance outflow boundary conditions. The latter guarantees a physiological intramural pressure level in the blood vessel [17, 41]. The inflow flowrate for the prestress problem may be selected so that the intramural pressure corresponds to the heart-cycle averaged pressure (about 85 mmHg).

Because (6) is a vector-valued equation with a tensor-valued unknown \mathbf{S}_0 , it, in principle, may have an infinite number of solutions. We obtain a particular solution for the state of prestress by means of the following procedure.

Starting with step $n = 1$, and setting $\mathbf{S}_0^n = \mathbf{0}$, we repeat the following steps:

1. Set $\mathbf{S}_0 = \mathbf{S}_0^n$ and $\mathbf{u} = \mathbf{0}$, which gives $\mathbf{F} = \mathbf{I}$ and $\mathbf{S} = \mathbf{0}$.
2. From $t_n \rightarrow t_{n+1}$, solve the following variational problem: Find \mathbf{u} , such that for all \mathbf{w} ,

$$\left(\mathbf{w}, \rho_0 \frac{\partial^2 \mathbf{u}}{\partial t^2} \right)_{\Omega_0^s} + (\nabla_X \mathbf{w}, \mathbf{F}(\mathbf{S} + \mathbf{S}_0))_{\Omega_0^s} + (\mathbf{w}, \tilde{\mathbf{h}})_{\Gamma_0^{fs}} = 0, \quad (7)$$

- where \mathbf{F} and \mathbf{S} are defined by Eqs. (2) and (4), respectively.
- Update $\mathbf{S}_0^{n+1} = \mathbf{S} + \mathbf{S}_0^n$ and increment n .

We continue the above iteration until $\mathbf{u} \rightarrow \mathbf{0}$. As a result, $\mathbf{F} \rightarrow \mathbf{I}$, $\mathbf{S} \rightarrow \mathbf{0}$, and we arrive at the solution of (6). It is important that we converge \mathbf{F} to the identity, because we would like to use Ω_0^s as the initial, undeformed configuration for FSI computations. In this case, the time-dependent FSI simulation departs from an equilibrium configuration, which is important for numerical stability. In Step 2, we advance the semi-discrete equations from t_n to t_{n+1} using the generalized- α time integrator [42].

Model	Inflow surface area (cm ²)
1	4.962×10^{-2}
2	2.102×10^{-2}

Table 1: Inflow cross-sectional areas for the aneurysm models.

Model	Fluid elements	Solid elements	Total elements	Total nodes
1	112,396	51,744	164,140	30,497
2	117,895	49,668	167,563	30,559

Table 2: Tetrahedral finite element mesh sizes for the aneurysm models.

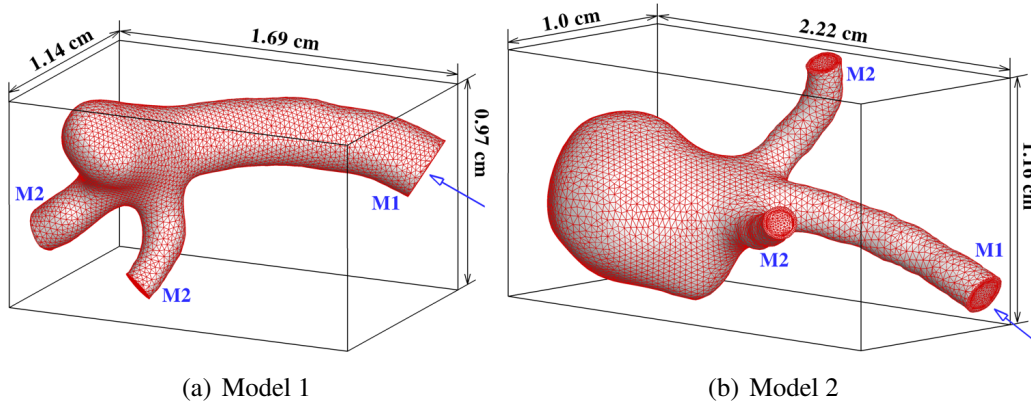


Figure 1: Tetrahedral finite element mesh of the middle cerebral artery (MCA) bifurcation with aneurysm. Inlet branches are labeled M1 and outlet branches are labeled M2 for both models. The arrows point in the direction of inflow velocity.

We apply our prestress procedure to two cerebral aneurysm models shown in Figure 1. The inflow and outflow branches are labeled as M1 and M2, respectively, in the same figure. Both models come from patient-specific imaging data and exhibit significant geometrical differences. Model 1 has a relatively small aneurysm

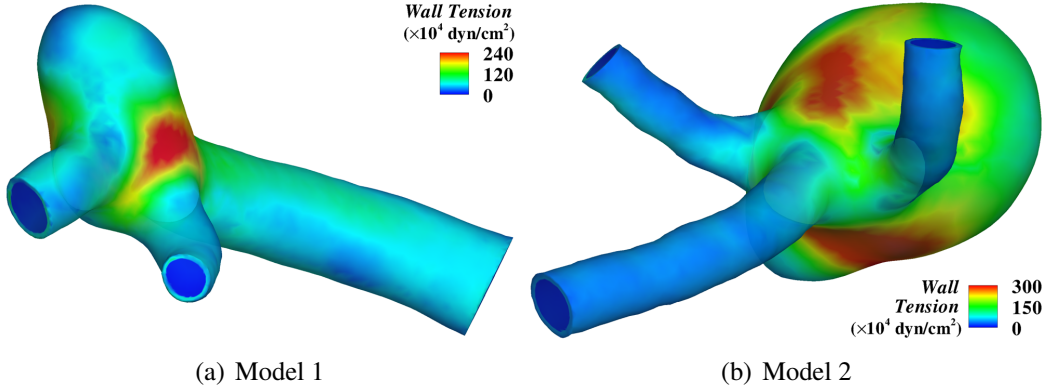


Figure 2: Final prestressed state for Model 1 and 2. The models are colored by the isocontours of wall tension, which is defined as the absolute value of the first principal in-plane stress of S_0 .

dome and an inlet branch of large radius. The situation is reversed for Model 2. Table 1 shows the inlet cross-sectional area for both models.

Meshing techniques developed by Zhang et al. [43] are used for generating linear tetrahedral elements for both models. The meshes contain both the blood flow volume and solid vessel wall. Fine meshes with boundary layer resolution are employed to ensure high fidelity of the computational results. The mesh sizes for both models are summarized in Table 2.

Figure 2 shows the final prestressed state for both models, which also demonstrates the applicability of the method to different vascular geometries. The models are colored by the isocontours of wall tension, which is defined as the absolute value of the first principal in-plane stress of S_0 .

2.3. Linearized elasticity operator

The linearization of the stress terms with respect to a displacement increment $\Delta \mathbf{u}$ in the conventional solid formulation given by (3) leads to the following bilinear form

$$\int_{\Omega_0} \nabla_X \mathbf{w} : \mathbf{D} \nabla_X \Delta \mathbf{u} d\Omega_0. \quad (8)$$

In the above, \mathbf{D} is the full tangent stiffness given by

$$\mathbf{D} = [D_{ijkl}], \quad (9)$$

$$D_{ijkl} = F_{il} C_{ijkl} F_{kk} + \delta_{ik} S_{jl}, \quad (10)$$

where $F_{il} C_{ijkl} F_{kk}$ is the material tangent stiffness and $\delta_{ik} S_{jl}$ is the geometrical tangent stiffness. C_{ijkl} are the components of the material elasticity tensor \mathbf{C} defined by

$$\mathbf{C} = 2 \frac{\partial \mathbf{S}}{\partial \mathbf{C}}. \quad (11)$$

Lower-case and upper-case indices are employed to denote the current and reference configuration quantities, respectively. The summation convention is employed on repeated indices and Cartesian basis is assumed throughout.

When the current configuration and reference configuration coincide (i.e. $\mathbf{x} = \mathbf{X}$), we have $\mathbf{S} = \mathbf{0}$ and $\mathbf{F} = \mathbf{I}$. Equation (10) becomes

$$\mathbf{D}_{IJKL} = \mathbf{C}_{IJKL}, \quad (12)$$

and only the material stiffness remains. Including the prestress tensor \mathbf{S}_0 into the solid model gives

$$D_{ijkl} = F_{ii}C_{IJKL}F_{kk} + \delta_{ik}(S_{jL} + S_{jL}^0), \quad (13)$$

where S_{jL}^0 are the components of \mathbf{S}_0 . For the case of $\mathbf{x} = \mathbf{X}$, we get

$$D_{IJKL} = C_{IJKL} + \delta_{IK}S_{jL}^0, \quad (14)$$

which means that the prestress is correctly accounted for in the geometrical stiffness.

2.4. Vascular FSI

The blood vessel wall is modeled as a three-dimensional hyperelastic solid in the Lagrangian description and has been detailed in the previous sections. The blood flow is governed by the Navier–Stokes equations of incompressible flow posed on a moving domain. The arbitrary Lagrangian–Eulerian (ALE) formulation is used, which is a popular choice for vascular blood flow applications [44–47]. Details and elaborations of the ALE formulation can be found, for example, in [17, 48].

At the interface between the blood flow and the elastic wall, velocity and traction compatibility conditions are assumed to hold. The motion of the fluid domain is governed by the equations of linear elasticity subject to Dirichlet boundary conditions coming from the time-dependent displacement of the fluid–solid interface [17, 49]. In the discrete setting this procedure is referred to as mesh motion.

The material parameters employed in this work are identical to those in [25]. Variable vessel wall thickness is considered in the modeling by performing a smooth Laplace operator-based extension of the inlet and outlet thickness data into the domain, which was a technique originally proposed in Bazilevs et al. [21]. In this work, the inlet and outlet vessel wall thickness is assumed to be 20% of their effective radii.

The solid and mesh motion equations are discretized using the Galerkin approach, while the fluid formulation makes use of the residual-based variational multiscale (RBVMS) method recently proposed by Bazilevs et al. [50]. The RBVMS methodology is built on the theory of stabilized and multiscale finite element methods (see, e.g. [51–54]). It applies equally well to laminar and turbulent flows and is thus attractive for applications where the nature of the flow solution is not known a priori.

The time-dependent discrete equations are solved using the generalized- α time integrator, which was originally proposed in Chung and Hulbert [42] and Jansen et al. [55] for structural dynamics and fluid mechanics, respectively, and further extended in Bazilevs et al. [17] for FSI. A monolithic solution strategy is adopted in which the increments of the fluid, solid, and mesh motion variables are obtained by means of a Newton–Raphson procedure in a simultaneous fashion. The effect of the mesh motion on the fluid equations is omitted from the tangent matrix for efficiency [18].

Simulations are driven by a prescribed time-periodic inlet velocity and outlet resistance boundary conditions. The inflow velocity profile can be found in [25]. The solid wall is subjected to zero traction boundary conditions at the outer surface. The inlet and outlet branches are allowed to slide in their cut planes as well as deform radially in response to the variations in the blood flow forces [25]. This gives more realistic arterial wall displacement patterns than fixed inlet and outlet cross-sections.

3. Computational results

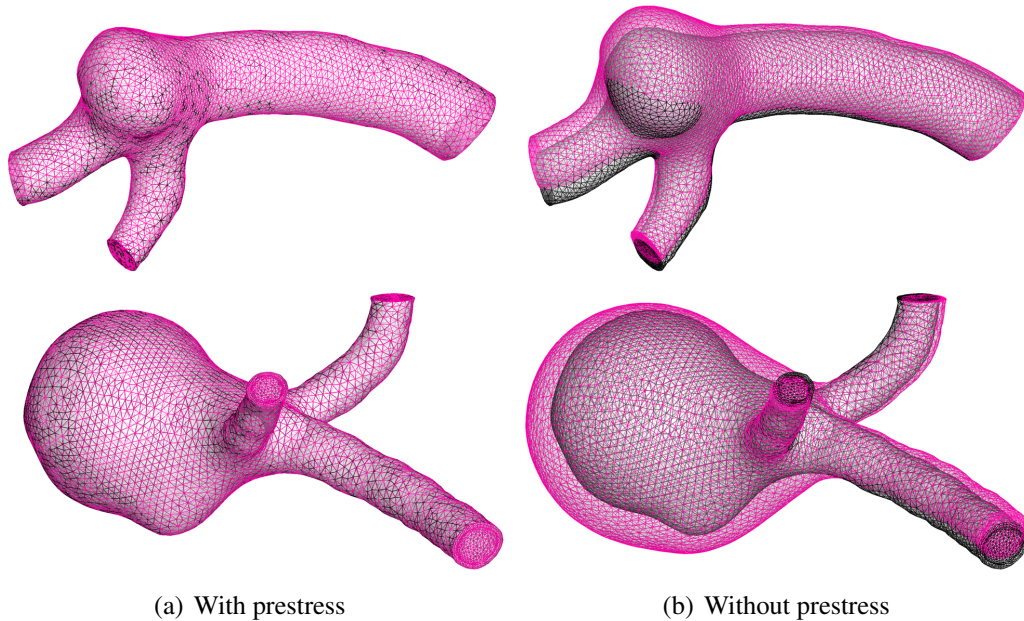


Figure 3: Relative wall displacement between the deformed configuration and reference configuration coming from imaging data. Top: Model 1; Bottom: Model 2. The deformed configuration corresponds to the time instant when the fluid traction vector is closest to the averaged traction vector used for the prestress problem (6).

To assess the influence of the prestress, we perform a coupled FSI simulation of both models and compare the results with and without prestress. Figure 3 shows the

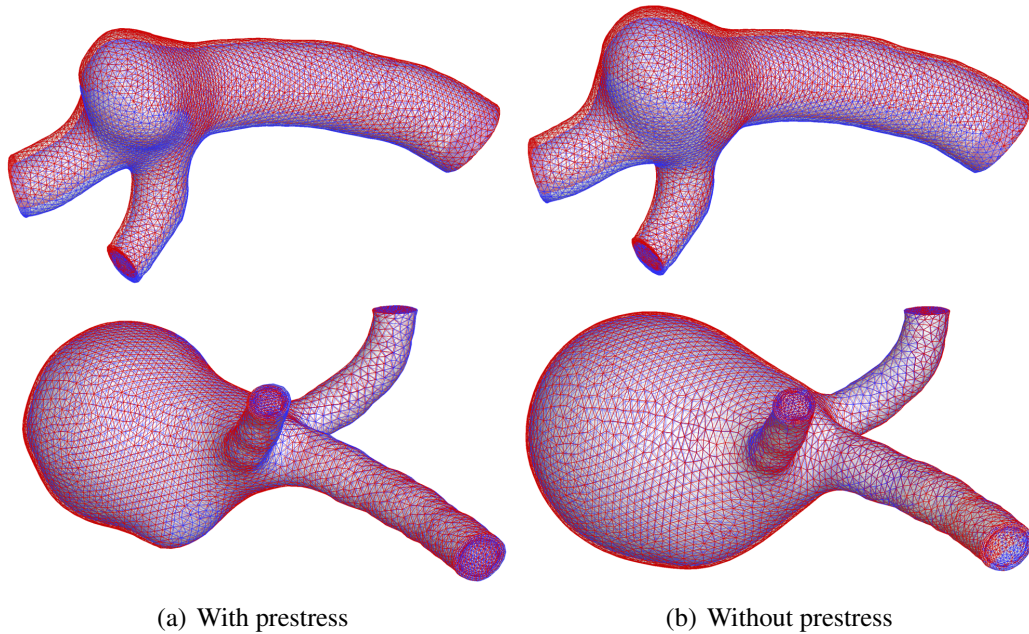


Figure 4: Relative wall displacement between the deformed configuration at peak systole and low diastole. Top: Model 1; Bottom: Model 2.

relative wall displacement between the deformed configuration and reference configuration coming from imaging data. The deformed configuration corresponds to the time instant when the fluid traction vector is closest to the averaged traction vector used for the prestress problem (6). Almost no difference between the reference and deformed configurations is seen in the case of the prestressed-artery simulation, as expected. However, in the case of non-prestressed simulation, the differences between the two configurations are significant. This indicates that the FSI problem is not being solved on the correct geometry. Furthermore, the relative geometry error is larger for Model 2, which has a larger aneurysm dome and a thinner wall. Figure 4 shows the relative wall displacement between the deformed configuration at peak systole and low diastole. In both the prestressed and non-prestressed cases the relative displacement is fairly small, yet non-negligible. The non-prestressed case, however, makes use of the geometry that is significantly more “inflated” compared to the prestressed case and the imaging data.

Figures 5 shows a comparison of the blood flow speed near peak systole for the simulations with and without prestress. The results between prestressed and non-prestressed cases are very similar, although some differences in the flow structures are visible, especially for Model 2. Figure 6 shows a comparison of the wall shear stress near peak systole for both cases. The wall shear stress, unlike blood flow velocity, exhibits significant differences in magnitude and spatial distribution. The wall tension results are shown in Figures 7. The wall tension is defined as the absolute value of the first principal in-plane stress (see [24] for details). Again, significant differences in magnitude and spatial distribution are observed. The com-

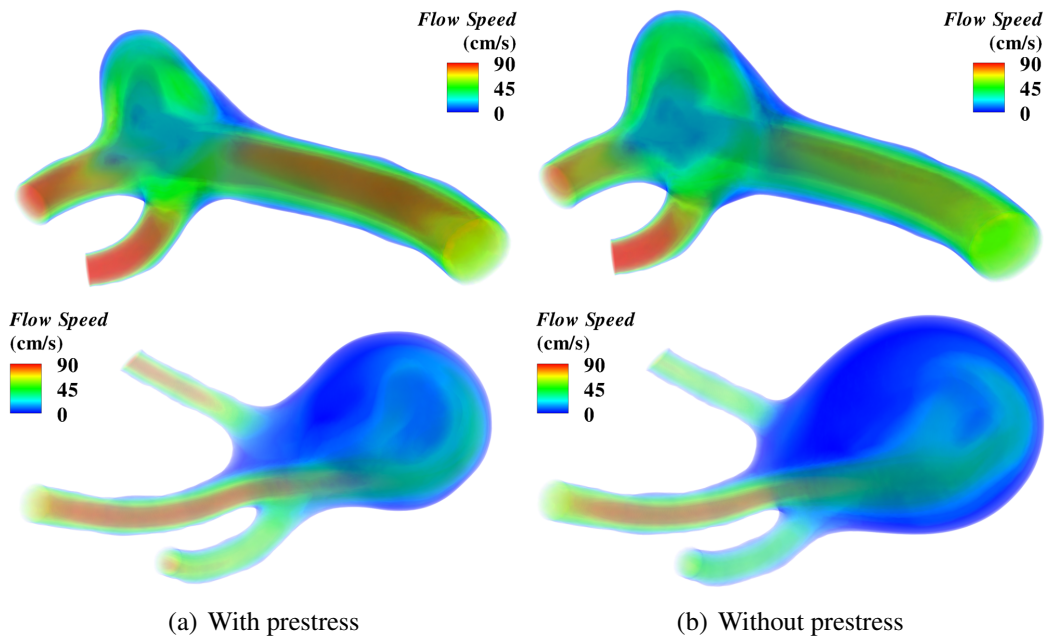


Figure 5: Volume-rendered blood flow velocity magnitude near peak systole. Top: Model 1; Bottom: Model 2.

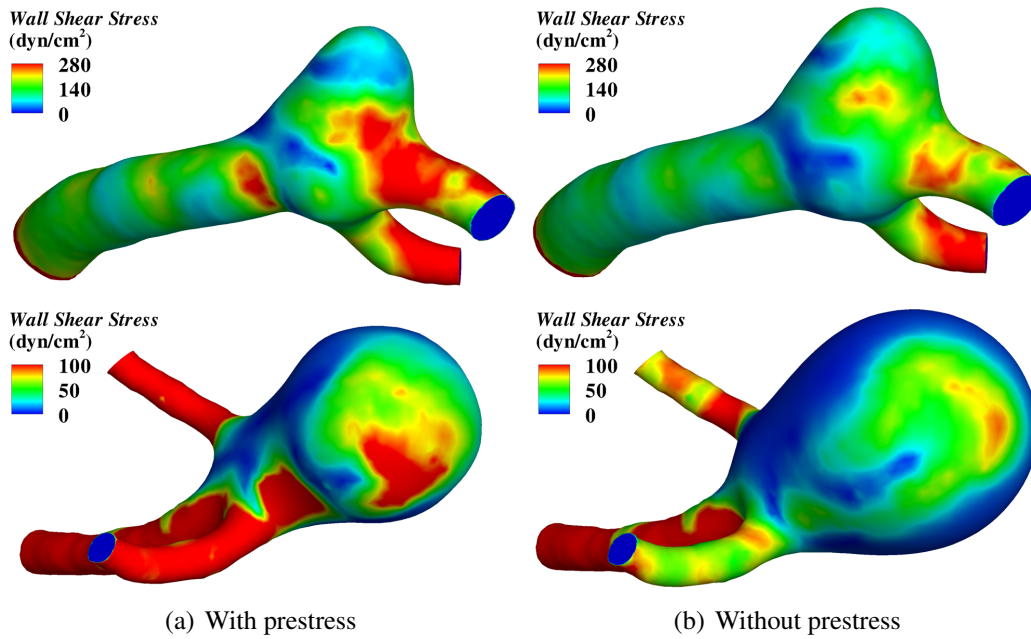


Figure 6: Wall shear stress near peak systole. Top: Model 1; Bottom: Model 2.

parisons clearly show the importance of considering prestress in the patient-specific vascular FSI simulations for accurate prediction of hemodynamic phenomena and vessel wall mechanics.

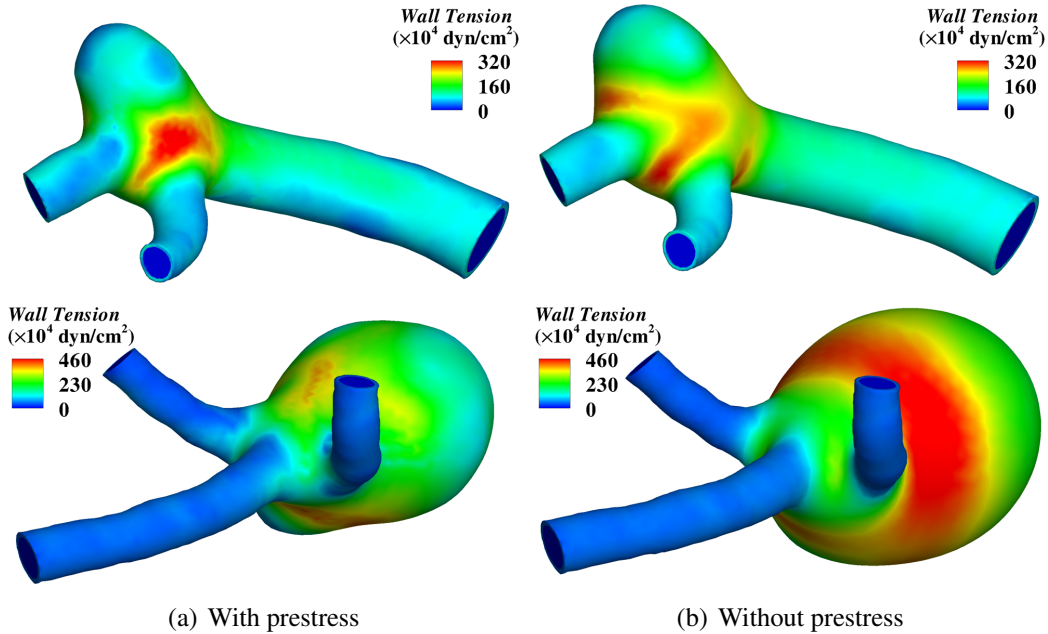


Figure 7: Wall tension near peak systole. Top: Model 1; Bottom: Model 2.

4. Conclusions

In this paper we proposed a blood vessel tissue prestress technique that allows us to correctly use the patient-specific geometry obtained from medical imaging data as reference geometry for vascular FSI computations. The technique consists of a simple iterative procedure that showed good convergence on patient-specific blood vessel models with very different geometry. We modified the solid modeling procedure to account for tissue prestress by employing an additive decomposition of the second Piola–Kirchhoff stress tensor. This decomposition gives a correct form of the tangent stiffness operator.

We employed the new solid formulation in the dynamic FSI analysis of two patient-specific cerebral aneurysm models and compared the results with the non-prestressed cases. We found that without prestress, the large intramural pressure tends to over-inflate the artery leading to significant discrepancies between imaging data and computational model geometry. This geometry error, in turn, produced large differences in the wall shear stress and wall tension. We conclude that pre-stressing is important in the FSI analysis of blood flow to accurately predict these quantities of hemodynamic interest.

Acknowledgement

We thank the Texas Advanced Computing Center (TACC) at the University of Texas at Austin for providing HPC resources that have contributed to the research results reported in this paper. We also thank SINTEF, ICT for partially supporting

this work. Prof. Tor Ingebrigtsen and Dr. Jorgen Isaksen of the Institute for Clinical Medicine, University of Tromsø, Norway and the Department of Neurosurgery, the University Hospital of North Norway provided us with patient-specific cerebral aneurysm data. Prof. Jessica Zhang and Wenyan Wang at Carnegie Mellon University provided us with meshes of the aneurysm models employed in this work. For this we are grateful.

References

- [1] A.M. Shaaban and André J. Duerinckx. Wall shear stress and early atherosclerosis: A review. *American Journal of Roentgenology*, 174:1657–1665, 2000.
- [2] D.M. Sforza, C.M. Putman, and J.R. Cebral. Hemodynamics of cerebral aneurysms. *Annual Review of Fluid Mechanics*, 41:91–107, 2009.
- [3] M.J. Levesque, D. Liepsch, S. Moravec, and R.M. Nerem. Correlation of endothelial cell shape and wall shear stress in a stenosed dog aorta. *Arteriosclerosis*, 6:220–229, 1986.
- [4] S. Kondo, N. Hashimoto, H. Kikuchi, F. Hazama, I. Nagata, and H. Kataoka. Cerebral aneurysms arising at nonbranching sites: An experimental study. *Stroke*, 28:398–404, 1997.
- [5] H. Meng, Z. Wang, Y. Hoi, L. Gao, E. Metaxa, D.D. Swartz, and J. Kolega. Complex hemodynamics at the apex of an arterial bifurcation induces vascular remodeling resembling cerebral aneurysm initiation. *Stroke*, 38:1924–1931, 2007.
- [6] M. Okano and Y. Yoshida. Junction complexes of endothelial cells in atherosclerosis-prone and atherosclerosis-resistant regions on flow dividers of brachiocephalic bifurcations in the rabbit aorta. *Biorheology*, 31:155–161, 1994.
- [7] M. Shojima, M. Oshima, K. Takagi, R. Torii, M. Hayakawa, K. Katada, A. Morita, and T. Kirino. Magnitude and role of wall shear stress on cerebral aneurysm: Computational fluid dynamic study of 20 middle cerebral artery aneurysms. *Stroke*, 35:2500–2505, 2004.
- [8] L. Boussel, V. Rayz, C. McCulloch, A. Martin, G. Acevedo-Bolton, M. Lawton, R. Higashida, W.S. Smith, W.L. Young, and D. Saloner. Aneurysm growth occurs at region of low wall shear stress: Patient-specific correlation of hemodynamics and growth in a longitudinal study. *Stroke*, 39:2997–3002, 2008.
- [9] C.A. Figueroa, I.E. Vignon-Clementel, K.E. Jansen, T.J.R. Hughes, and C.A. Taylor. A coupled momentum method for modeling blood flow in three-dimensional deformable arteries. *Computer Methods in Applied Mechanics and Engineering*, 195:5685–5706, 2006.

- [10] B.J.B.M. Wolters, M.C.M. Rutten, G.W.H. Schurink, U. Kose, J. de Hart, and F.N. van de Vosse. A patient-specific computational model of fluid–structure interaction in abdominal aortic aneurysms. *Medical Engineering & Physics*, 27:871–883, 2005.
- [11] Y. Bazilevs, V.M. Calo, Y. Zhang, and T.J.R. Hughes. Isogeometric fluid-structure interaction analysis with applications to arterial blood flow. *Computational Mechanics*, 38:310–322, 2006.
- [12] R. Torii, M. Oshima, T. Kobayashi, K. Takagi, and T.E. Tezduyar. Influence of the wall elasticity in patient-specific hemodynamic simulations. *Computers and Fluids*, 36:160–168, 2007.
- [13] R. Torii, M. Oshima, T. Kobayashi, K. Takagi, and T.E. Tezduyar. Computer modeling of cardiovascular fluid-structure interactions with the deforming-spatial-domain/stabilized space-time formulation. *Computer Methods in Applied Mechanics and Engineering*, 195:1885–1895, 2006.
- [14] R. Torii, M. Oshima, T. Kobayashi, K. Takagi, and T.E. Tezduyar. Fluid-structure interaction modeling of aneurysmal conditions with high and normal blood pressures. *Computational Mechanics*, 38:482–490, 2006.
- [15] C.M. Scotti and E.A. Finol. Compliant biomechanics of abdominal aortic aneurysms: A fluid–structure interaction study. *Computers & Structures*, 85:1097–1113, 2007.
- [16] T.E. Tezduyar, S. Sathe, T. Cragin, B. Nanna, B.S. Conklin, J. Pausewang, and M. Schwaab. Modelling of fluid-structure interactions with the space-time finite elements: Arterial fluid mechanics. *International Journal for Numerical Methods in Fluids*, 54:901–922, 2007.
- [17] Y. Bazilevs, V.M. Calo, T.J.R. Hughes, and Y. Zhang. Isogeometric fluid-structure interaction: theory, algorithms, and computations. *Computational Mechanics*, 43:3–37, 2008.
- [18] Y. Bazilevs, J.R. Gohean, T.J.R. Hughes, R.D. Moser, and Y. Zhang. Patient-specific isogeometric fluid-structure interaction analysis of thoracic aortic blood flow due to implantation of the Jarvik 2000 left ventricular assist device. *Computer Methods in Applied Mechanics and Engineering*, 198:3534–3550, 2009.
- [19] R. Torii, M. Oshima, T. Kobayashi, K. Takagi, and T.E. Tezduyar. Fluid-structure interaction modeling of a patient-specific cerebral aneurysm: influence of structural modeling. *Computational Mechanics*, 43:151–159, 2008.
- [20] R. Torii, M. Oshima, T. Kobayashi, K. Takagi, and T.E. Tezduyar. Fluid-structure interaction modeling of blood flow and cerebral aneurysm: Significance of artery and aneurysm shapes. *Computer Methods in Applied Mechanics and Engineering*, 198:3613–3621, 2009.

- [21] Y. Bazilevs, M.-C. Hsu, D.J. Benson, S. Sankaran, and A.L. Marsden. Computational fluid–structure interaction: Methods and application to a total cavopulmonary connection. *Computational Mechanics*, 45:77–89, 2009.
- [22] K. Takizawa, J. Christopher, T.E. Tezduyar, and S. Sathe. Space–time finite element computation of arterial fluid–structure interactions with patient-specific data. *International Journal for Numerical Methods in Biomedical Engineering*, 26:101–116, 2010.
- [23] P. Rissland, Y. Alemu, S. Einav, J. Ricotta, and D. Bluestein. Abdominal aortic aneurysm risk of rupture: Patient-specific FSI simulations using anisotropic model. *Journal of Biomechanical Engineering*, 131:031001, 2009.
- [24] Y. Bazilevs, M.-C. Hsu, Y. Zhang, W. Wang, X. Liang, T. Kvamsdal, R. Brekken, and J. G. Isaksen. A fully-coupled fluid–structure interaction simulation of cerebral aneurysms. *Computational Mechanics*, 46:3–16, 2010.
- [25] Y. Bazilevs, M.-C. Hsu, Y. Zhang, W. Wang, T. Kvamsdal, S. Hentschel, and J.G. Isaksen. Computational vascular fluidstructure interaction: methodology and application to cerebral aneurysms. *Biomechanics and Modeling in Mechanobiology*, 9:481–498, 2010.
- [26] K. Takizawa, C. Moorman, S. Wright, J. Christopher, and T.E. Tezduyar. Wall shear stress calculations in space–time finite element computation of arterial uid–structure interactions. *Computational Mechanics*, 46:31–41, 2010.
- [27] K. Takizawa, C. Moorman, S. Wright, J. Purdue, T. McPhail, P.R. Chen, J. Warren, and T.E. Tezduyar. Patient-specific arterial fluid–structure interaction modeling of cerebral aneurysms. *International Journal for Numerical Methods in Fluids*, 2010. Published online, 10.1002/flid.2360.
- [28] J.G. Isaksen, Y. Bazilevs, T. Kvamsdal, Y. Zhang, J.H. Kaspersen, K. Waterloo, B. Romner, and T. Ingebrigtsen. Determination of wall tension in cerebral artery aneurysms by numerical simulation. *Stroke*, 39:3172–3178, 2008.
- [29] C.A. Taylor and J.D. Humphrey. Open problems in computational vascular biomechanics: Hemodynamics and arterial wall mechanics. *Computer Methods in Applied Mechanics and Engineering*, 198:3514–3523, 2009.
- [30] G.A. Holzapfel. *Nonlinear Solid Mechanics, A Continuum Approach for Engineering*. Wiley, Chichester, 2000.
- [31] J.D. Humphrey. *Cardiovascular Solid Mechanics, Cells, Tissues, and Organs*. Springer, New York, 2002.
- [32] T.E. Tezduyar, S. Sathe, M. Schwaab, and B.S. Conklin. Arterial fluid mechanics modeling with the stabilized space-time fluid-structure interaction technique. *International Journal for Numerical Methods in Fluids*, 57:601–629, 2008.

- [33] M.W. Gee, C. Reeps, H.H. Eckstein, and W.A. Wall. Prestressing in finite deformation abdominal aortic aneurysm simulation. *Journal of Biomechanics*, 42:1732–1739, 2009.
- [34] M.W. Gee, Ch. Förster, and W.A. Wall. A computational strategy for prestressing patient-specific biomechanical problems under finite deformation. *International Journal for Numerical Methods in Biomedical Engineering*, 26:52–72, 2010.
- [35] S. Govindjee and P.A. Mihalic. Computational methods for inverse finite elastostatics. *Computer Methods in Applied Mechanics and Engineering*, 136:47–57, 1996.
- [36] P.W. Alford, J.D. Humphrey, and L.A. Taber. Growth and remodeling in a thick-walled artery model: effects of spatial variations in wall constituents. *Biomechanics and Modeling in Mechanobiology*, 7:245–262, 2008.
- [37] S. Baek, K.R. Rajagopal, and J.D. Humphrey. A theoretical model of enlarging intracranial fusiform aneurysms. *Journal of Biomechanical Engineering*, 128:142–149, 2006.
- [38] C.A. Figueroa, S. Baek, C.A. Taylor, and J.D. Humphrey. A computational framework for fluid-solid-growth modeling in cardiovascular simulations. *Computer Methods in Applied Mechanics and Engineering*, 198:3583–3602, 2009.
- [39] J.C. Simo and T.J.R. Hughes. *Computational Inelasticity*. Springer-Verlag, New York, 1998.
- [40] S. Lipton, J.A. Evans, Y. Bazilevs, T. Elguedj, and T.J.R. Hughes. Robustness of isogeometric structural discretizations under severe mesh distortion. *Computer Methods in Applied Mechanics and Engineering*, 199:357–373, 2009.
- [41] I.E. Vignon-Clementel, C.A. Figueroa, K.E. Jansen, and C.A. Taylor. Outflow boundary conditions for three-dimensional finite element modeling of blood flow and pressure in arteries. *Computer Methods in Applied Mechanics and Engineering*, 195:3776–3796, 2006.
- [42] J. Chung and G.M. Hulbert. A time integration algorithm for structural dynamics with improved numerical dissipation: The generalized- α method. *Journal of Applied Mechanics*, 60:371–375, 1993.
- [43] Y. Zhang, W. Wang, X. Liang, Y. Bazilevs, M.-C. Hsu, T. Kvamsdal, R. Brekken, and J.G. Isaksen. High-fidelity tetrahedral mesh generation from medical imaging data for fluid-structure interaction analysis of cerebral aneurysms. *Computer Modeling in Engineering & Sciences*, 42:131–150, 2009.
- [44] L. Formaggia, J.F. Gerbeau, F. Nobile, and A. Quarteroni. On the coupling of 3D and 1D Navier-Stokes equations for flow problems in compliant vessels. *Computer Methods in Applied Mechanics and Engineering*, 191:561–582, 2001.

- [45] J.-F. Gerbeau, M. Vidrascu, and P. Frey. Fluid–structure interaction in blood flows on geometries based on medical imaging. *Computers and Structures*, 83:155–165, 2005.
- [46] M.A. Fernández, J.-F Gerbeau, A. Gloria, and M. Vidrascu. A partitioned Newton method for the interaction of a fluid and a 3D shell structure. Technical Report RR-6623, INRIA, 2008.
- [47] S. Badia, F. Nobile, and C. Vergara. Robin-Robin preconditioned Krylov methods for fluid-structure interaction problems. *Computer Methods in Applied Mechanics and Engineering*, 198:2768–2784, 2009.
- [48] M.A. Fernández and J.-F. Gerbeau. Algorithms for fluid–structure interaction problems. In L. Formaggia, A. Quarteroni, and A. Veneziani, editors, *Cardiovascular Mathematics: Modeling and simulation of the circulatory system*, chapter 9. Springer, 2009.
- [49] A.A. Johnson and T.E. Tezduyar. Mesh update strategies in parallel finite element computations of flow problems with moving boundaries and interfaces. *Computer Methods in Applied Mechanics and Engineering*, 119:73–94, 1994.
- [50] Y. Bazilevs, V.M. Calo, J.A. Cottrell, T.J.R. Hughes, A. Reali, and G. Scovazzi. Variational multiscale residual-based turbulence modeling for large eddy simulation of incompressible flows. *Computer Methods in Applied Mechanics and Engineering*, 197:173–201, 2007.
- [51] A.N. Brooks and T.J.R. Hughes. Streamline upwind/Petrov-Galerkin formulations for convection dominated flows with particular emphasis on the incompressible Navier-Stokes equations. *Computer Methods in Applied Mechanics and Engineering*, 32:199–259, 1982.
- [52] T.E. Tezduyar. Stabilized finite element formulations for incompressible flow computations. *Advances in Applied Mechanics*, 28:1–44, 1992.
- [53] T.E. Tezduyar and Y. Osawa. Finite element stabilization parameters computed from element matrices and vectors. *Computer Methods in Applied Mechanics and Engineering*, 190:411–430, 2000.
- [54] T.J.R. Hughes, G. Scovazzi, and L.P. Franca. Multiscale and stabilized methods. In E. Stein, R. de Borst, and T.J.R. Hughes, editors, *Encyclopedia of Computational Mechanics, Vol. 3: Fluids*, chapter 2. Wiley, 2004.
- [55] K.E. Jansen, C.H. Whiting, and G.M. Hulbert. A generalized- α method for integrating the filtered Navier-Stokes equations with a stabilized finite element method. *Computer Methods in Applied Mechanics and Engineering*, 190:305–319, 1999.